Conformation and Dynamics of Atactic Poly(acrylonitrile). 1. Trans/Gauche Ratio from Double-Quantum Solid-State ^{13}C NMR of the Methylene Groups

Hironori Kaji† and Klaus Schmidt-Rohr*

Department of Polymer Science and Engineering, University of Massachusetts, Amherst, Massachusetts 01003

Received February 11, 2000; Revised Manuscript Received April 28, 2000

ABSTRACT: The trans/gauche ratio of backbone bonds in atactic poly(acrylonitrile) (aPAN) was characterized by several two-dimensional solid-state NMR experiments, using 15% $^{13}CH_2$-carbon labeled aPAN. An estimate of the conformational ratio was obtained from a double-quantum filtered NMR experiment, which correlates the $^{13}C-^{13}C$ internuclear vector of two adjacent $^{13}CH_2$ groups with their ^{13}C chemical shift anisotropies. The orientation of the chemical shift tensor was determined in auxiliary experiments. The backbone conformation of two successive bonds was characterized by double-quantum NMR spectroscopy, which correlates the orientation-dependent ^{13}C chemical shifts of two adjacent $^{13}CH_2$ segments. The experiments were performed with and without $^{13}C-^{13}C$ dipolar decoupling. From the three two-dimensional NMR spectra that were obtained, the trans/gauche ratio of aPAN was determined as 90%:10% (±10%). This value is compatible with the previously reported experimental density and wide-angle X-ray diffraction patterns of aPAN. The high trans content is also consistent with the single CH_2 resonance line observed under magic-angle spinning.

1. Introduction

The elucidation of the microscopic structure of solid polymers is one of the important goals in polymer science, since the establishment of the relationships between structure and properties is crucial for the design of novel materials. The crystal structures of many polymers have been determined by wide-angle X-ray diffraction (WAXD), but some of them are still controversial because the crystalline state is chemically (configurationally) and/or physically (conformationally) disordered.[1]

Commercial poly(acrylonitrile) (PAN) is produced by radical polymerization, and the tacticity is atactic.[2−4] Due to the configurational disorder, most atactic vinyl polymers with bulky side groups, for example poly(styrene), poly(methyl methacrylate), poly(vinyl acetate), and related systems, cannot crystallize and remain amorphous. In contrast, poly(vinyl alcohol), poly(vinyl chloride), and poly(vinyl fluoride) have relatively small side groups and are able to crystallize.[1,5] Atactic poly(acrylonitrile) (aPAN) is also a crystallizable polymer, despite its larger C≡N side group. The crystal structure is, however, disordered due to the configurational disorder and is not well understood.[6−36]

WAXD patterns of oriented aPAN fibers show two relatively sharp reflections along the equator, indicating laterally ordered chain packing with a nearest chain-to-chain distance of 6.0 Å.[6,9,11,20,28] In contrast, only diffuse patterns appear along the meridian and in the quadrants. Several models of the crystal structure have been proposed to explain the WAXD patterns. Bohn et al.[9] suggested that aPAN is a laterally ordered polymer with little or no longitudinal order. Lindenmeyer and Hosemann[11] proposed the theory of paracrystals in order to explain the WAXD patterns of solution-grown single crystals of aPAN. Liu and Ruland[20] suggested the existence of about one kink per 10 monomer units in a planar trans zigzag conformation, while Rizzo et al.[28] searched for possible low-energy conformations without invoking a kink formation, using a conformational analysis of energetically optimized model chains. They proposed a model in which torsion angles are close to 180° in racemo dyads and deviate significantly from 180° in meso dyads. All these crystal-structure models rely only on the WAXD patterns and density measurements.[9,32−34] Additional microscopic experimental data that can shed light on the backbone conformation of aPAN are necessary to reveal the crystal structure of aPAN.

Recent developments of solid-state NMR techniques enable us to analyze torsion angles and their distributions in unoriented organic solids. For instance, a two-dimensional chemical shift anisotropy (2D CSA) spin-diffusion technique has offered detailed information on local structures, and its potential has been demonstrated by structure determination of not only crystalline but also glassy materials.[37−50] However, the trans state or parallel segments, which frequently appear in the conformation of polymers, often cannot be detected by this technique because their signals are hidden by the diagonal ridge in the 2D spectrum. Thus, quantitative analyses of torsion angle distributions are impossible by this technique. Our 2D double-quantum spectroscopy (DOQSY) technique[51−57] can solve this problem, since it can detect all relative orientations, including parallel segments and the trans state. Therefore, the trans/gauche ratio in polymers can be quantified.[54,55,57]

In this article, the trans/gauche ratio in aPAN is analyzed. For this purpose, we apply three different solid-state NMR techniques to a 15% $^{13}CH_2$-carbon-labeled aPAN ($^{13}CH_2$-aPAN) sample, as shown in Figure 1. The first is a double-quantum-filtered 2D experiment correlating the $^{13}C-^{13}C$ dipolar interaction with the ^{13}C CSA (DQF-CC/CSA experiment). This probes the direction of the $^{13}C-^{13}C$ internuclear vector in the principal-axes system (PAS) of the CSA and thus provides the

* To whom correspondence should be addressed at: Department of Chemistry, Iowa State University, Ames, IA 50011. E-mail srohr@iastate.edu.

† On leave from the Institute for Chemical Research, Kyoto University, Uji, Kyoto, 611-0011, Japan.

10.1021/ma0002592 CCC: $19.00
Published on Web 06/23/2000

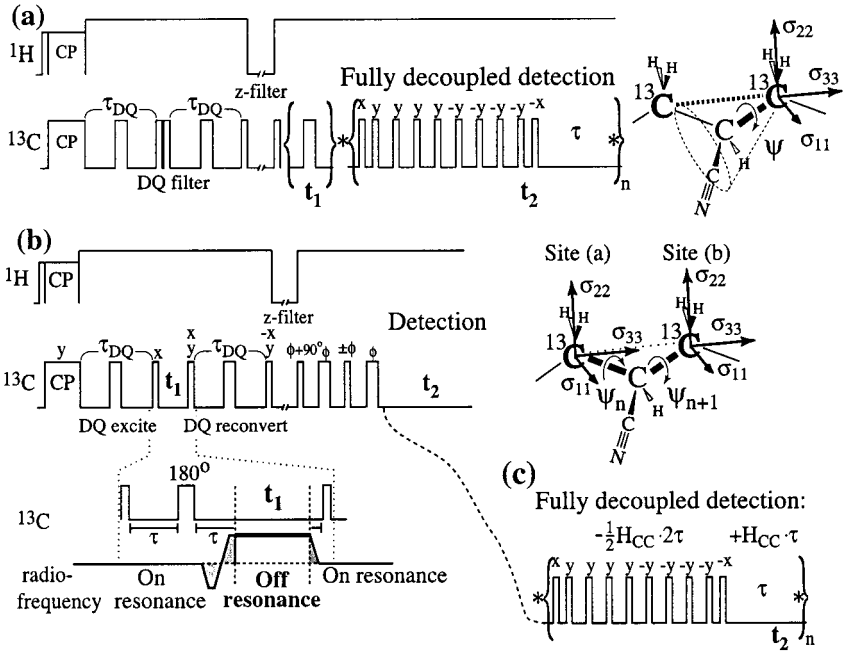

Figure 1. Pulse sequences and schematic representations of (a) the DQ-filtered CC/CSA experiment with fully decoupled detection, (b) the DOQSY experiment without $^{13}C-^{13}C$ dipolar decoupling (DQ/CSA+CC spectrum), and (c) the DOQSY experiment with $^{13}C-^{13}C$ dipolar decoupling in the detection period (DQ/CSA spectrum).

torsion angle of one backbone bond attached to the $^{13}CH_2$ group as shown in Figure 1. To simplify the spectrum, the $^{13}C-^{13}C$ dipolar interaction in the detection period is decoupled by a multiple-pulse sequence.[53] A DQ filter is applied in order to suppress the large, undesirable isolated-spin signals, which appear in the 2D spectrum at $\omega_1 = 0$. Second, a 2D DOQSY experiment, which correlates the sum of two chemical shift frequencies (double-quantum (DQ) coherence) with the individual frequencies (single-quantum (SQ) coherence), provides information on the torsion angles of the two successive bonds between two labeled $^{13}CH_2$ sites. This experiment is performed in two variants: (i) with $^{13}C-^{13}C$ dipolar decoupling during the t_2 acquisition period (DQ/CSA experiment) and (ii) without $^{13}C-^{13}C$ dipolar decoupling during acquisition, so that the line shape in ω_2 reflects both the CSA and the dipolar coupling (DQ/CSA+CC experiment). Third, a one-dimensional (1D) ^{13}C spectrum under magic angle spinning (MAS) and ^1H dipolar decoupling is recorded to examine the conformation-dependent isotropic chemical shifts based on the γ-gauche effect. Finally, the results are compared with previous experiments and with models of aPAN. The measurement of precise trans torsion angles and their distributions for trans−trans meso and racemo dyads will be discussed in our following article.[58]

2. Experimental Section

2.1. Samples. A powdered aPAN sample labeled with 15% of $^{13}CH_2$ carbon was prepared by slurry radical polymerization of acrylonitrile (AN) in aqueous solution with a REDOX catalyst.[59] The two-necked round-bottomed flask with 20 mL of deaerated distilled water, 0.375 mL of $^{13}CH_2$-labeled AN, and 2.125 mL of unlabeled AN equipped with a stirrer, a rubber septum, and a reflux condenser was placed into a water bath at 55 °C. Nitrogen (N_2) gas flow was applied from the top of the condenser. A solution of 1 mL of water containing 0.2 mL of 0.1 N H_2SO_4 and 0.06 mg of $(NH_4)Fe(SO_4)_2 \cdot 6H_2O$ was added through the septum. After the contents of the flask reached 55 °C (~30 min), 1.25 mL of water containing 5 mg of $K_2S_2O_8$ and 1.25 mL of water containing 25 mg of $NaHSO_3$ were added quickly through the septum. The reaction continued for 1 h under stirring. The as-polymerized white aPAN was washed by an excess amount of water, followed by drying under vacuum for 1 day. The dried powder sample was annealed at 100 °C for 3 min under N_2 gas flow. A yield of 66% was obtained. In this polymerization, AN was not distilled, to avoid loss of labeled AN. We confirmed by WAXD as well as ^{13}C and ^1H solution NMR experiments that aPAN samples polymerized from distilled and undistilled AN showed no differences. It is also stated in ref 59 that a distillation is not necessary for the polymerization of aPAN.

2.2. Sample Characterization. The intrinsic viscosity (in dimethylformamide) at 60 °C was 1.54 dL g^{-1} and corresponded to a viscosity-average molecular weight of 1.2×10^5, calculated by an intrinsic viscosity−molecular weight relation, $[\eta] = 3.35 \times 10^4 M_w^{0.72}$.[60,61] The triad tacticity measured by solution ^{13}C NMR was *mm*:*mr*:*rr* = 29:50:21 from CH (α-) carbon resonance lines. WAXD patterns for the powdered aPAN samples gave a relatively sharp main reflection at $2\theta = 17.0 \pm 0.2°$ with a full width at half-maximum (fwhm) of 1.6° and a small reflection at around 29.4°. These reflections correspond to $\xi = 0.19$ and 0.33 $Å^{-1}$ (Miller indices of (100) and (110), respectively), indicating that our sample is laterally packed in a pseudohexagonal form with a smallest interchain distance of $a = b = \sim 6.0$ Å. A broad reflection centered at around $2\theta \approx 26°$ was also observed. These WAXD observations are in agreement with the most commonly reported polymorph.[6,9,11,20,28]

2.3. NMR Measurements. The solid-state NMR experiments were performed on a Bruker DSX-300 spectrometer in a magnetic field of 7.0 T. The sample was inserted as a cylindrical block into the 4.5 mm coil of a stationary Bruker double-resonance probe. Pulse sequences used in this paper are shown in Figures 1 and 2. Typical experimental parameters for 2D experiments are as follows. The ^1H and ^{13}C 90° pulse lengths were 2.6 and 2.2 μs, respectively. A cross-polarization time of 1 ms was used except for the experiment correlating the $^1H-^1H$ dipolar coupling with the CSA (HH/CSA experiment). A recycle delay of 3−6 s, a *z*-filter before detection of 0.5 ms, and an acquisition time of 5.12 ms were used. The window τ in the Hahn−solid−Hahn echo[53] was 20−24 μs. The dwell time during detection was 20 μs except for the fully decoupled experiments. ^1H decoupling fields $\gamma B_1/2\pi$ of 140−160 kHz were used. All the experiments were carried

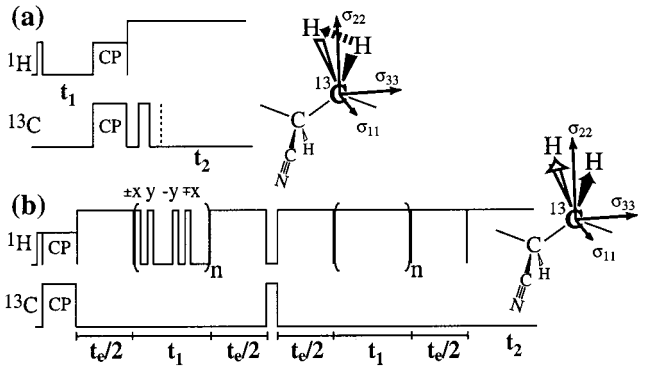

Figure 2. Pulse sequences and schematic representations of the relevant couplings in (a) the HH/CSA experiment and (b) the CH/CSA experiment, which are used for determining the orientation of the CH_2 ^{13}C chemical shift tensor.

out at ambient temperature. Cosine data sets were measured off resonance in ω_1 and processed to yield purely absorptive, nonquadrature spectra. Further parameters are given for each experiment below.

In our previous and forthcoming studies of semicrystalline polymers,[51,62] a T_1 or $T_{1\rho}$ filter is applied if the crystalline component is to be studied selectively. For all the experiments in this paper, however, we measured all the components in aPAN, without using any filters for the selection of certain morphological components. The relaxation time filtering was avoided because the phase structure of aPAN is not yet well understood, as will be discussed below and in this series of papers.[63]

2.3.1. 2D HH/CSA and CH/CSA Experiments. At first, the chemical shift tensor orientation of the $^{13}CH_2$ carbon should be determined experimentally, since this CSA is used for torsion angle determination in the following experiments. The chemical shift tensor orientation of the $^{13}CH_2$ carbon can be determined from a 2D HH/CSA experiment and a 2D experiment correlating the $^{13}C-^1H$ dipolar couplings with the CSA (CH/CSA experiment) of $^{13}CH_2$-aPAN. Pulse sequences for these experiments are shown in Figure 2. For the HH/CSA experiment, a contact time for CP of 24 μs was used to select an isolated $^1H-^1H$ dipolar coupling of $^1H-^{13}C-^1H$ sites. Twelve slices with increments of 5 μs were acquired with 256 scans for each t_1 slice. For the CH/CSA experiment, a ^1H 90° pulse length of 2.2 μs was used during MREV-8 homonuclear decoupling.[64,65] The echo delay t_e (see Figure 2) was set to 1 ms. Twenty-four slices with increments of 22.2 μs were acquired with 384 scans per t_1 slice. Total acquisition times for these experiments were 3−7 h.

The following principles permit to understand the information contained in an HH/CSA spectrum; detailed descriptions of the technique are given in refs 66−70. The orientation-dependent homonuclear dipolar frequency is given by

$$\omega_D^{II} = 1.5\delta_D^{II}\frac{1}{2}(3\cos^2\theta - 1) \quad (1)$$

with

$$\delta_D^{II} = -\frac{\mu_0}{4\pi}\hbar\frac{\gamma^2}{r_{II}^3} = 2\pi \times 120\ \text{kHz}\frac{1}{(r_{II}/\text{Å})^3} \quad (2)$$

Here, θ is the angle between the H−H internuclear vector and the static magnetic field $\mathbf{B}_0$, and r_{II} is the distance between these two protons. This equation shows that the strongest dipolar interaction is obtained when $\theta = 0°$, and the weakest interaction is obtained when $\theta = 54.7°$ (magic angle). A local maximum in the magnitude is obtained when $\theta = 90°$. In a CSA spectrum, a resonance line appears at the chemical shift principal value σ_{nn} when the direction of the nth principal axis of the chemical shift tensor $\underline{\sigma}$ is parallel to B_0. Thus, from 2D HH/CSA spectra, the polar coordinates (α, β) of the internuclear H−H vector in the PAS of the chemical shift tensor can be determined. The largest line width in the ω_1 dimension is obtained for the CSA tensor direction parallel to the H−H vector, the smallest when the two directions make an angle of 54.7°, which is also half of the bond angle of a sp^3-hybridized carbon.

Similarly, in the ω_1 dimension of a CH/CSA spectrum, the CH heteronuclear dipolar frequency is given by the D_{zz} element of the dipolar interaction tensor in the laboratory frame for a C−H system:[70]

$$\omega_D^{IS} = \frac{1}{2}D_{zz} = \delta_D^{IS}\frac{1}{2}(3\cos^2\theta - 1) \quad (3)$$

with

$$\delta_D^{IS} = -\frac{\mu_0}{4\pi}\hbar\frac{\gamma_I\gamma_S}{r_{IS}^3} = 2\pi \times 30\ \text{kHz}\frac{1}{(r_{IS}/\text{Å})^3} \quad (4)$$

where θ is the angle between the C−H internuclear vector and $\mathbf{B}_0$ and r_{IS} is the C−H bond length. During MREV-8 homonuclear decoupling in Figure 2b, the S (^{13}C) spin in a C−H group evolves under the heteronuclear dipolar interaction given by eqs 3 and 4 producing an NMR signal of

$$s(t) = \cos(\omega_D^{IS}t) = {}^1/_2\exp(i\omega_D^{IS}t) + {}^1/_2\exp(-i\omega_D^{IS}t) \quad (5)$$

Therefore, the spectrum for a given θ consists of a doublet at $+\omega_D^{IS}(\theta)$ and $-\omega_D^{IS}(\theta)$, such that the splitting is $2\omega_D^{IS}(\theta)$. For a CH_2 group, there are two C−H bonds: $C-H^A$ and $C-H^B$. The time signal then becomes

$$s(t) = \cos(\omega_D^{IS(A)}t)\cos(\omega_D^{IS(B)}t) = {}^1/_2\cos\{(\omega_D^{IS(A)} + \omega_D^{IS(B)})t\} + {}^1/_2\cos\{(\omega_D^{IS(A)} - \omega_D^{IS(B)})t\} \quad (6)$$

In this case, it is convenient to consider, and diagonalize, the "element dipolar tensors" $\boldsymbol{D^S} = \boldsymbol{D^A} + \boldsymbol{D^B}$ (sum) and $\boldsymbol{D^D} = \boldsymbol{D^A} - \boldsymbol{D^B}$ (difference). For the "sum tensor" $\boldsymbol{D^S}$, the $D^S{}_{11}$ principal axis is parallel to the H−H internuclear vector, the $D^S{}_{22}$ axis along the H−C−H bisector, and the $D^S{}_{33}$ axis perpendicular to the H−C−H plane.[67−70] The 2D CH/CSA spectrum for a CH_2 group correlates the PAS of the $C-H_2$ dipolar sum tensor with that of the chemical shift tensor through the Euler angles (α', β', γ'). The ^{13}C chemical shift tensor orientation is determined by this experiment, since the $C-H_2$ dipolar sum tensor in the CH_2 group is well-known as described above.

2.3.2. 2D DQF-CC/CSA and DQ/CSA(+CC) Experiments. 2D DQF-CC/CSA and DQ/CSA(+CC) experiments on $^{13}CH_2$-aPAN were carried out to determine the trans/gauche ratio in aPAN. Pulse sequences for these experiments are shown in Figure 1. DQ excitation and reconversion delays of τ_{DQ} = 0.4 ms (τ_{DQ} corresponds to 2τ in our previous papers[51,53−55,57]) were used in these experiments. The ^{13}C frequency was switched 4.5 kHz off-resonance during the evolution time t_1 in order to separate the DQ signals from SQ and zero quantum artifacts.[71] Each switching time was 6−12 μs. All the pulses were applied on resonance, i.e., at a frequency near the center of the CSA spectrum. For fully decoupled detection, a ^{13}C 90° pulse length of 2.4 μs was used, and 80 data points with an effective dwell time of 40 μs were sampled. In the DQF-CC/CSA experiment, 16 t_1 slices with increments of 417.6 μs were acquired with 640 scans per slice. In DQ/CSA(+CC) experiments, 80 t_1 slices with increments of 20 μs were acquired with 256 scans per slice. Total acquisition times for these three spectra were 17 h (DQF-CC/CSA), 23 h (DQ/CSA+CC), and 34 h (DQ/CSA).

3. Background

3.1. Designation of Torsion Angles. In this paper, we follow the IUPAC designation for torsion angles.[72] Torsion angles are defined in the range $-180° < \psi < 180°$. Conformations with torsion angles within ±30°

from ±180° (trans), ±120° (anticlinal), ±60° (gauche), and 0° (cis) are indicated by the symbols *T*, *A*, *G*, and *C*, respectively. This designation is different from Flory's where the torsion angle of trans is defined as 0°.[73,74] In the case of vinyl polymers, two gauche conformations with backbone torsion angles of +60° and −60° give different conformations. To distinguish these conformations, we follow the designation described originally in refs 1 and 72−75 and used in our previous paper.[55] The symbol $\bar{G}$ corresponds to the conformation with the three bulky substituents, namely the CN group and the two main chain "continuations", close to each other. This $\bar{G}$ conformation is assigned a torsion angle of ca. −60°. (This agrees with ref 75 but is opposite in sign compared to ref 55, which is in turn more consistent with the polystyrene literature.) The symbol *G* corresponds to the conformation with the opposite sign, +60°. The $\bar{G}$ conformation is more unfavorable than *G* due to larger steric hindrance. The conformations of *GG* and $G\bar{G}$ sequences are also unfavorable due to steric crowding, the so-called "pentane effect".[74,75]

Similarly, other torsion angles of opposite signs are also used to designate sterically inequivalent conformations; for instance, +120° and −120° are sterically different and termed *A* and $\bar{A}$. Furthermore, we will refer to the torsion angles of ±160°, ±140°, ±100°, and ±20° as $T'/\bar{T}'$, $A'/\bar{A}'$, $A''/\bar{A}''$, and $C'/\bar{C}'$, respectively.

3.2. Effect of Molecular Reorientations. To examine the contribution of molecular reorientation, additional 2D CSA exchange experiments were carried out on a ^{15}N-labeled aPAN sample. The ^{15}N CSA is a good probe for main-chain dynamics. No off-diagonal signals are observed with a mixing time of 5 ms at 20 °C. This confirms that the contribution of motion is negligibly small for the 2D DQF and DOQSY experiments, since the total time of DQ reconversion and *z*-filter periods, 0.9 ms, is even shorter than 5 ms. The detailed investigation of the dynamics of aPAN will be published later in this series of papers.[63]

3.3. Statistics of ^{13}C Labeling and Long-Distance Correlations. In 2D DOQSY spectra, only the signals of ^{13}C spin pairs are desirable, while single ^{13}C spins and sequences of three or more ^{13}C spins produce unwanted backgrounds or artifacts. Unlike in doubly labeled samples,[51,53,54,62] ^{13}C's are statistically distributed in the present case, which produces various spin sequences with different number of ^{13}C's. Thus, we should minimize the effects of isolated ^{13}C spins and of three-spin (and longer) sequences. The detailed treatment of the statistics of ^{13}C-labeled sites and effects of longer spin sequences have been described in our previous paper,[55] so only some modifications are discussed here.

For the pulse sequences of 2D DQ/CSA+CC and DQ/CSA, the radio-frequency jump is applied before and after the DQ evolution as described above (see Figure 1).[71] Switching the frequency off-resonance in ω_1 permits a complete separation of the DQ spectrum from zero-quantum and single-quantum artifacts, while all the pulses are applied on-resonance. Thus, the crucial artifacts that we should consider are due to DQ coherences of three or more spins. The fraction of isolated sequences of *n* spins is calculated as[55]

$$r_n(x) = nx^{n-1}(1-x)^2 \tag{7}$$

where *x* is the fraction of labeled sites. Thus, the ratio of the fraction of isolated sequences of three or more spins to the fraction of isolated spin pairs is given by

$$\frac{\sum_{n=3}^{\infty} r_n(x)}{r_2(x)} = \frac{1-\sum_{n=1}^{2} r_n(x)}{r_2(x)} = \frac{x(3-2x)}{2(1-x)^2} \tag{8}$$

For small *x*, this reduces to ∼1.5*x*. The $^{13}CH_2$-labeling level of 15% chosen here is lower than in our previous work on atactic polystyrene (aPS),[55] where a 24% $^{13}CH_2$-labeled polymer was used. By reducing the labeled percentage from 24% to 15%, the fraction of sequences of three or more spins relative to that of isolated spin pairs is reduced significantly, from 0.52 to 0.28. While a detailed discussion of the multispin DQ patterns is beyond the scope of this paper, it is worth noting that the undesirable DQ coherences that involve three or more spins significantly give relatively small,[55] negative[76] signals, in particular at short τ_{DQ}. In fact, at the short excitation and reconversion time τ_{DQ} of 0.4 ms, three-spin systems behave as independent pairs of two-spin systems to a good approximation.[55] The effect of four or more spins is expected to be negligible.

3.4. Intermolecular Correlation. In our experiments, intermolecular ^{13}C−^{13}C correlations might be suspected to affect the spectrum, since all the chains are 15% ^{13}C-labeled. Fortunately, the intramolecular 2.52 Å distance between ^{13}C sites separated by two bonds is significantly shorter than the intermolecular chain-to-chain distance of 6.0 Å in aPAN;[6,9,11,20,28] this distance is indeed relevant since the methylene groups will be located near the centers of the chains. Therefore, we can neglect intermolecular ^{13}C−^{13}C correlations and can observe intramolecular ^{13}C−^{13}C correlations selectively. Within the relatively short DQ excitation time of τ_{DQ} = 0.4 ms, the DQ excitation efficiency of intermolecular couplings is only ∼1% of that of a 2.52 Å two-bond coupling.[55]

4. Results and Discussion

4.1. Determination of the CSA Tensor Orientation from HH/CSA and CH/CSA Spectra. Figure 3a shows the experimental HH/CSA spectrum of the methylene groups in $^{13}CH_2$-aPAN. It provides information on the ^{13}C chemical shift tensor orientation with respect to the chemical bonds, by specifying the orientation of the H−H internuclear vector relative to the ^{13}C chemical shift PAS.

In the HH/CSA spectrum of Figure 3a, the widest resonance lines in ω_1 are obtained at the left edge of the spectrum in the second dimension, $\omega_2 = \sigma_{11}$. This result indicates that the H−H vector is almost along the σ_{11} axis. The local maximum in the ω_1 width at σ_{33} suggests that the σ_{33} direction is perpendicular to the H−H vector. The narrowest resonance lines in ω_1 are obtained between σ_{22} and σ_{33} for the HH/CSA experiment. This feature is the same as for the CH_2 carbon in polyethylene (PE), whose σ_{11} axis is along the H−H internuclear vector, the σ_{22} axis along the H−C−H bisector, and the σ_{33} axis perpendicular to the H−C−H plane.[68,69,77,78]

Figure 4a displays the CH/CSA spectrum of $^{13}CH_2$-aPAN, which correlates the chemical shift tensor orientation with the directions of the C−H bonds. The spectrum in Figure 4a is dominated by a narrow peak at $\omega_2 = \sigma_{22}$, near the center of the spectrum. This

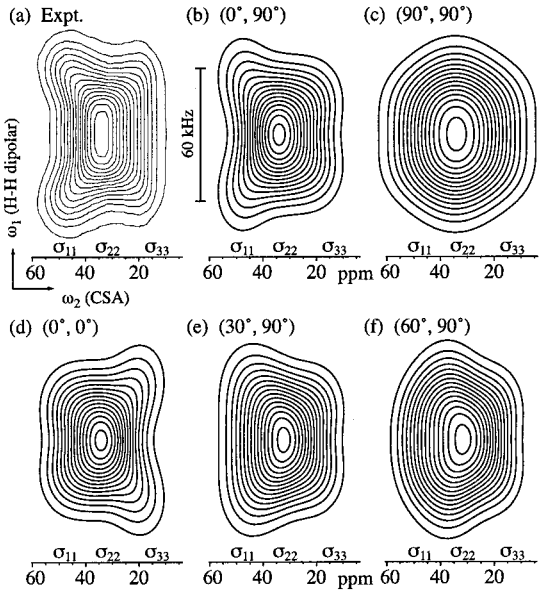

Figure 3. 2D ^{1}H−^{1}H dipolar/^{13}C chemical shift anisotropy spectra of $^{13}CH_2$-aPAN (HH/CSA spectra). (a) Experimental spectrum. (b)−(f) Simulated spectra with different chemical shift tensor orientations. The polar coordinates of the H−H internuclear vector in the PAS of the CSA (see Figure 2a) are given in each figure. The fixed parameters were $\sigma_{11} = 50.5$ ppm, $\sigma_{22} = 34.5$ ppm, $\sigma_{33} = 16.5$ ppm, $r_{CH} = 1.09$ Å, and ∠H−C−H = 109.5°. Gaussian broadenings with full widths at half-height of 9 kHz and 6 ppm were applied in the ω_1 and ω_2 dimensions, respectively. Fifteen contour lines were plotted between 6.5% and 97% of the maximum intensity.

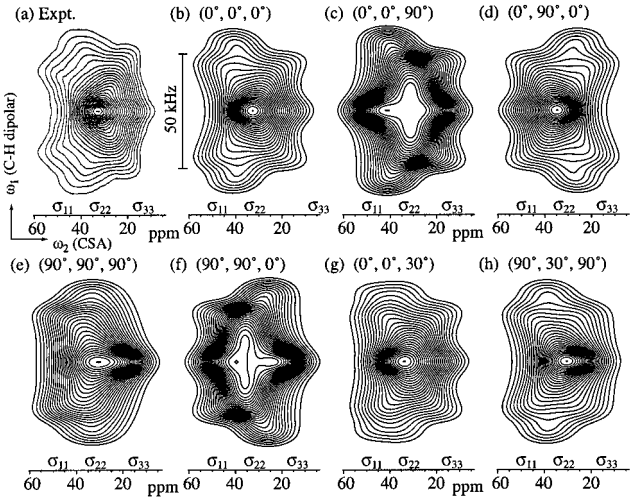

Figure 4. 2D ^{13}C−^{1}H dipolar/^{13}C chemical shift anisotropy spectra of $^{13}CH_2$-aPAN (CH/CSA spectra). (a) Experimental spectrum. (b)−(h) Simulated spectra with different chemical shift tensor orientations. The Euler angles that specify the relative orientation of the PAS of the dipolar sum tensor (see text) and the PAS of the CSA are given in each figure. The fixed CSA and bonding parameters were the same as listed in the caption of Figure 3. Gaussian broadenings with full widths at half-height of 3 kHz and 7 ppm were applied in the ω_1 and ω_2 dimensions, respectively. Twenty-eight contour lines were plotted between 6.9% and 99.8% of the maximum intensity.

indicates that the direction of the central chemical shift principal value, σ_{22}, is along the $D^S{}_{22}$ principal axis of the dipolar sum tensor, that is, along the H−C−H bisector. It is also seen that two nearly straight, mirror symmetric ridges run from σ_{11} to σ_{33}, indicating that the dipolar sum tensor PAS and the chemical shift PAS are essentially parallel. Additional broadened intensity appears from σ_{11} to σ_{22} and the central intensity (at $\omega_1 = 0$) at σ_{33}. This pattern originates from the "difference tensor" $\boldsymbol{D^D}$, whose $D^D{}_{11}$ and $D^D{}_{33}$ principal axes are disposed symmetrically ±45° from the H−C−H bisector, while the $D^D{}_{22}$ axis is perpendicular to the H−C−H plane.[67−70] Thus, the direction of σ_{33} is found to be along $D^D{}_{22}$, that is, perpendicular to the H−C−H plane. This also confirms the above assignment of the chemical shift tensor orientation.

To verify this analysis, simulated spectra for these experiments are shown in Figure 3b−f and Figure 4b−h. In Figure 3, the orientation is specified in terms of only two Euler angles (α, β) as described above, because a γ-rotation of the PAS of the chemical shift tensor around the H−H vector does not change their orientational relation. Figure 3b corresponds to the same chemical shift tensor orientation as in PE. In parts c and d of Figure 3, the directions of (σ_{11}, σ_{22}) and of (σ_{11}, σ_{33}), respectively, are interchanged relative to Figure 3b. The resulting patterns are clearly different from the experimental spectrum. The interchange of (σ_{22}, σ_{33}), of (σ_{11}, σ_{33}), and of (σ_{11}, σ_{22}) from parts b, c, and d of Figure 3, respectively, gives the same spectrum of the corresponding original spectrum. Figure 3e,f indicates that rotations around the σ_{33} axis by more than ±30° result in significant deviations from the experimental spectrum.

Figure 4b shows the simulated CH/CSA spectrum whose chemical shift tensor orientation is the same as for PE. In parts c, d, and e of Figure 4, the directions of (σ_{11}, σ_{22}), of (σ_{11}, σ_{33}), and of (σ_{22}, σ_{33}), respectively, are interchanged relative to Figure 4b. In Figure 4f, the directions of (σ_{11}, σ_{33}) are interchanged relative to Figure 4c. The spectrum whose directions of (σ_{11}, σ_{33}) are interchanged from Figure 4e gives a pattern similar to the mirror image of Figure 4e (not shown here). This spectrum and the spectra in (c)−(f) are clearly different from the experimental spectrum. Figure 4g,h indicates that 30° rotations around the σ_{33} and σ_{11} axes give deviations from the experimental spectrum. An even clearer difference is observed for a rotation around the σ_{22} axis. From these two experiments, it is concluded that the chemical shift tensor orientation is the same as in polyethylene within uncertainties of ±20°. The same result was obtained previously for atactic polystyrene.[55]

It is difficult to determine the chemical shift PAS directions more accurately, because detailed features of these 2D HH/CSA and CH/CSA spectra are smeared out by strong inhomogeneous line broadening. The line width (fwhm) of $^{13}CH_2$-aPAN estimated from a 1D CP/MAS spectrum is 485 Hz (6.4 ppm). This large line width must be attributed to the disordered local structure of aPAN, including conformational, configurational, and packing disorder. The ^{13}C−^{13}C dipolar interactions may also increase the line width, but the ^{13}C labels are unavoidable; they are required to make the CH signal insignificant, which overlaps with the CH_2 resonance line. The chemical shift tensor orientation and the principal values of the CH_2 carbon in meso and racemo dyads can be expected to be somewhat different due to the influence of the C≡N side groups.

The spectra show clear indications of different distributions of the three principal values; in particular, a stronger inhomogeneous broadening near σ_{11} is observed. To keep the calculation time manageable, in the simulations the distributions were approximated by

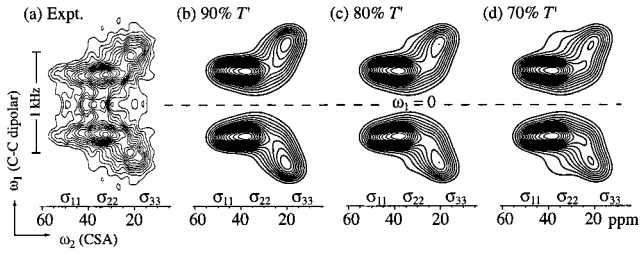

Figure 5. 2D double-quantum filtered $^{13}C-^{13}C$ dipolar/^{13}C chemical shift anisotropy spectra of $^{13}CH_2$-aPAN with $^{13}C-^{13}C$ dipolar decoupling and $\tau_{DQ} = 0.4$ ms (DQF-CC/CSA spectra). (a) Experimental spectrum. (b)−(d) Simulated spectra with T':G ratios of (b) 90:10; (c) 80:20, and (d) 70:30. In the simulations, torsion angles of ±160° and ±60° were used for trans and gauche conformations, respectively. Gaussian broadenings with full widths at half-height of 4 Hz and 3 ppm were applied in the ω_1 and ω_2 dimensions, respectively. Fifteen contour lines were plotted between 11.8% and 94.1% of the maximum intensity.

three values for each principal value: $\sigma_{11} = 41.5$, 50.5, and 59.5 ppm; $\sigma_{22} = 29.5$, 34.5, and 39.5 ppm; and $\sigma_{33} = 14.5$, 16.5, and 18.5 ppm. The resulting isotropic chemical shift is 33.8 ± 3.5 ppm.

4.2. Conformation Measurements. 4.2.1. DQF-CC/CSA Experiment. Figure 5a shows the experimental DQF-CC/CSA spectrum of $^{13}CH_2$-aPAN. The $^{13}C-^{13}C$ dipolar coupling in the ω_1 dimension is correlated with the pure CSA in ω_2. While CC/CSA spectra of ^{13}C-pair labeled polymers have been measured without a DQ filter,[46,79,80] for the statistically $^{13}CH_2$-labeled aPAN a DQ filter is required to suppress the artifact at $\omega_1 = 0$ that arises from the isolated spins; this undesired sharp ridge would otherwise dominate the spectrum, prevent the measurement of small dipolar couplings, and introduce truncation artifacts even for $\omega_1 \neq 0$. The total duration of the DQ filter used was $2\tau_{DQ} = 0.8$ ms.

In the spectrum of Figure 5a, the $^{13}C-^{13}C$ dipolar widths at σ_{11} and σ_{22} are quite similar, and that at σ_{33} is wider than those at σ_{11} and σ_{22}. As explained above, this indicates that the $^{13}C-^{13}C$ internuclear vector is nearly along the σ_{33} direction and perpendicular to σ_{11} and σ_{22} directions (see eq 1). The chemical structure of aPAN in Figure 1a shows that this geometrical relation corresponds to a backbone conformation close to trans.

4.2.2. DQ/CSA Experiment. Figure 6a shows the experimental DQ/CSA spectrum of $^{13}CH_2$-aPAN with $\tau_{DQ} = 0.4$ ms. The signal intensity appears along the diagonal of slope two in the 2D spectrum. This shows that the dominant backbone conformation is close to trans. The slope-two diagonal corresponds to the condition of $\omega_a = \omega_b$,[81] since the spectrum correlates the sum frequency $\omega_a + \omega_b$ of the two dipolar-coupled ^{13}C nuclei (see Figure 1b) with the single-quantum frequency, ω_a or ω_b, in the ω_2-dimension.

4.2.3. DQ/CSA+CC Experiment. Figure 7a shows the experimental DQ/CSA+CC spectrum of $^{13}CH_2$-aPAN with $\tau_{DQ} = 0.4$ ms. As in the DQ/CSA spectrum, the signal intensity appears generally along the diagonal of slope two, indicating again that the backbone conformation is predominantly in a state close to trans. In this experiment, however, the signal intensity along the diagonal of slope two is split into doublets of varying splitting in the ω_2 dimension, due to $^{13}C-^{13}C$ dipolar couplings with a maximum strength of $\nu_D = \pm 470$ Hz. The spectrum is also modulated by the DQ excitation/reconversion efficiency.[51,55,57]

In cases of directly bonded $^{13}C-^{13}C$ pairs, such as in $^{13}CH_2-^{13}CH_2$ doubly labeled PE or poly(ethylene terephthalate) (PET),[51,53,54] large $^{13}C-^{13}C$ dipolar couplings of up to $\nu_D = \pm 3$ kHz make it difficult to distinguish trans and gauche conformations. In those cases, the $^{13}C-^{13}C$ dipolar decoupled version of the DQ/CSA experiment is preferable. In the present case, however, the dipolar coupled spectrum is worth recording, in addition to the dipolar decoupled version. The labeled ^{13}C sites of $^{13}CH_2$-aPAN sample are separated by two bonds, and the dipolar coupling strength is smaller than that for directly bonded $^{13}C-^{13}C$ in PE and PET.[51,53,54] This smaller strength of the couplings reduces the complications they produce, and we can determine the backbone conformation in aPAN by a $^{13}C-^{13}C$ dipolar coupled version of the experiment as already shown for aPS.[55] The $^{13}C-^{13}C$ dipolar coupled version spectrum exhibits some specific features that are important for the torsion angle determination. Details will be described in the next section.

4.3. Simulations. To extract detailed information on the backbone conformation from the three experimental 2D DQF and DQ spectra shown above, we compare them to simulated 2D spectra for various possible conformations. The chemical shift principal axes directions were determined by the CH/CSA and HH/CSA

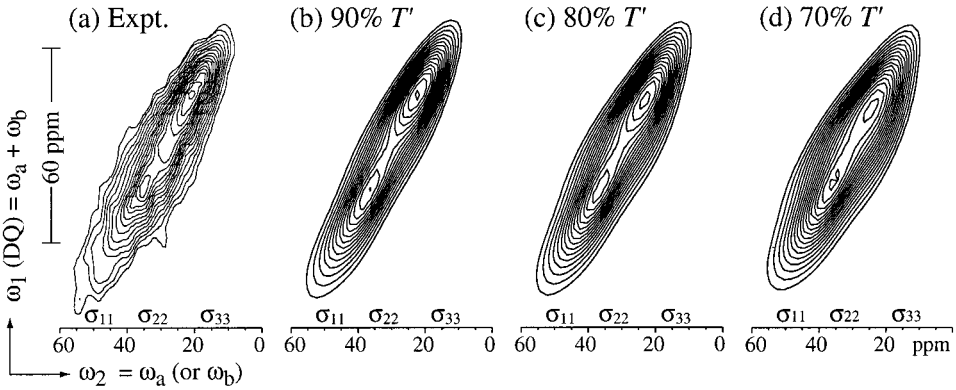

Figure 6. 2D ^{13}C double-quantum/chemical shift anisotropy spectra of $^{13}CH_2$-aPAN with $^{13}C-^{13}C$ dipolar decoupling, for $\tau_{DQ} = 0.4$ ms (DQ/CSA spectra). (a) Experimental spectrum. (b)−(d) Simulated spectra with (b) $T'T'$:$T'G = 80$:20 (trans content of 90%), (c) $T'T'$:$T'G = 60$:40 (trans content of 80%), and (d) $T'T'$:$T'G = 40$:60 (trans content of 70%). For these simulations, only gauche conformations in the $T'G$ conformation were considered; any types of GG conformations were not included. For all the simulations, torsion angles of ±160° and ±60° were used for trans and gauche conformations, respectively. Gaussian broadenings with full widths at half-height of 8 and 2 ppm were applied along and perpendicular to the diagonal of slope two, respectively. Seventeen contour lines were plotted between 15.5% and 98% of the maximum intensity.

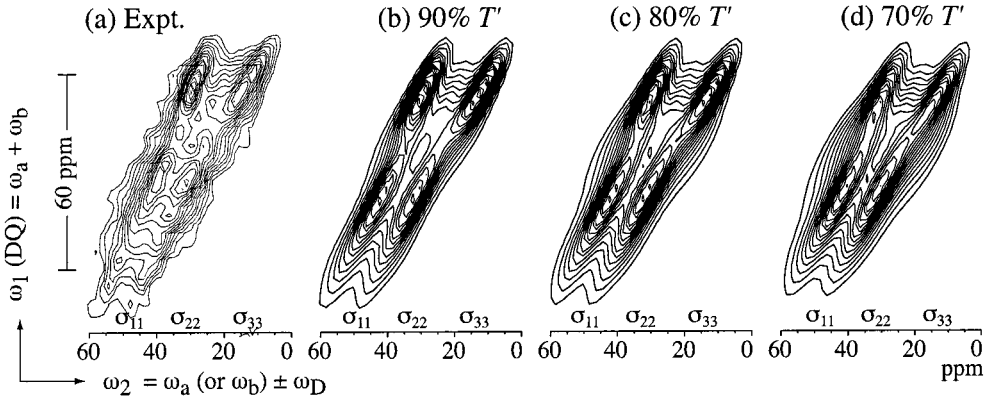

Figure 7. 2D ^{13}C double-quantum/chemical shift anisotropy spectra of $^{13}CH_2$-aPAN without $^{13}C-^{13}C$ dipolar decoupling and τ_{DQ} = 0.4 ms (DQ/CSA+CC spectra). (a) Experimental spectrum. (b)−(d) Simulated spectra with (b) $T'T'$:$T'G$ = 80:20 (trans content of 90%), (c) $T'T'$:$T'G$ = 60:40 (trans content of 80%), and (d) $T'T'$:$T'G$ = 40:60 (trans content of 70%). For these simulations, only the $T'G$ conformation was considered as the gauche conformation; any types of GG conformations were not included. In all the simulations, torsion angles of ±160° and ±60° were used for trans and gauche conformations, respectively. Gaussian broadenings with full widths at half-height of 6 and 1.4 ppm were applied along and perpendicular to the diagonal of slope two, respectively. Sixteen contour lines were plotted between 11.6% and 99% of the maximum intensity.

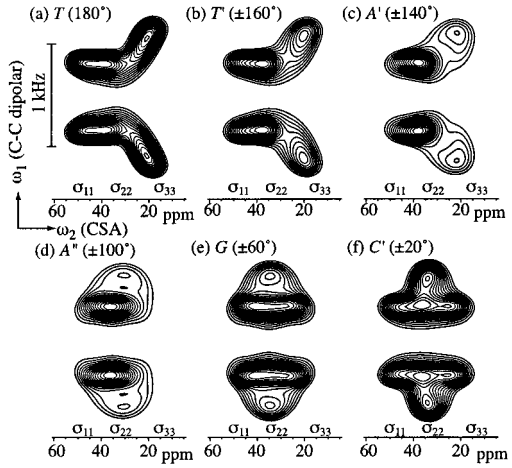

Figure 8. Simulated 2D double-quantum filtered $^{13}C-^{13}C$ dipolar/^{13}C chemical shift anisotropy (DQF−CC/CSA) spectra of $^{13}CH_2$-aPAN, with $^{13}C-^{13}C$ dipolar decoupling during detection, for various conformations. The torsion angle values are indicated above each spectrum. Note that in this figure, for simplicity, T' is used to indicate T' or $\bar{T}'$, A' stands for A' or $\bar{A}'$, and C' stands for C' or $\bar{C}'$. Parameters for simulations and plotting are the same as in Figure 5.

experiments as discussed above. In the simulations, the DQ excitation/reconversion modulation and intermediate $^{13}C-^{13}C$ dipolar coupling are calculated analytically.[51,57,82]

4.3.1. DQF-CC/CSA Simulation. Figure 8 shows simulated 2D DQF-CC/CSA spectra for some typical torsion angles. A strong dependence of the 2D spectra on the torsion angle is clearly observed, and we can thus distinguish trans and gauche conformations. Simulations for trans conformations give the largest splitting in the $^{13}C-^{13}C$ dimension at $\omega_2 = \sigma_{33}$. In contrast, for gauche conformations the largest splitting in the $^{13}C-^{13}C$ dimension appears around $\omega_2 = \sigma_{22}$. By comparing the experimental spectrum with these simulations, the dominant conformation is found to be trans. Among trans conformations, a torsion angle of ±160° gives a suitable simulated spectrum. In contrast, the simulated spectra for anticlinal, gauche, and cis conformations in Figure 8 are clearly different from the experimental spectrum.

Figure 5b−d shows simulations with trans contents of 90%−70%; torsion angles of ±160° and ±60° were used for trans and gauche conformations, respectively. Although the simulation with a trans content of 90% gives the best fit and that with a trans content of 70% exhibits smaller intensity at $\omega_2 = \sigma_{33}$, the difference is not particularly pronounced. Thus, from this experiment we can only conclude semiquantitatively that the backbone conformation of aPAN is predominantly trans.

4.3.2. DQ/CSA Simulation. Figure 9 shows simulated 2D DQ/CSA spectra for some typical conformations. Here, we can obtain information on two successive torsion angles since 2D DQ/CSA spectra depend on two successive torsion angles. As observed in Figure 9, trans and gauche conformations can be distinguished by this experiment. In contrast to trans conformations, whose spectra extend along the diagonal of slope two, gauche conformations give intensity near the center of the 2D plane. Some torsion angles, such as (160°, 160°) and (−160°, −160°), or (60°, 60°) and (−60°, −60°), cannot be distinguished because they are geometrically equivalent. However, if only one of the signs is changed, from (160°, 160°) to (160°, −160°), or from (60°, 60°) to (60°, −60°), the spectra are different. Note that the assignments of parts h and i of Figure 9 to $GG/\bar{G}\bar{G}$ and $G\bar{G}$, respectively, are corrected compared to similar simulations in ref 55. Also, while TG and $T\bar{G}$ yield the same spectra, the $T'\bar{G}$ and $T'G$ patterns in Figure 9f,g are slightly different. Consistent with the 2D DQF-CC/CSA experiment, simulations with torsion angles of (±160°, ±160°) for the trans−trans conformations give the best agreement with the experimental spectrum.

Figure 6b−d shows simulations with trans contents of 90%−70%, with torsion angles of (±160°, ±160°) and (160°, 60°) for trans−trans and trans−gauche conformations, respectively. The simulation with a trans content of 90% gives the best fit, while the simulated spectrum with a trans content of 70% is wider than the experimental spectrum. Therefore, we can conclude that the trans content in aPAN is 90% (±10%).

4.3.3. DQ/CSA+CC Simulation. Figure 10 shows simulated 2D DQ/CSA+CC spectra. The torsion angles are the same as in the corresponding spectra in Figure 9, and the torsion angle symmetry properties are also identical. The spectral patterns are now affected by the

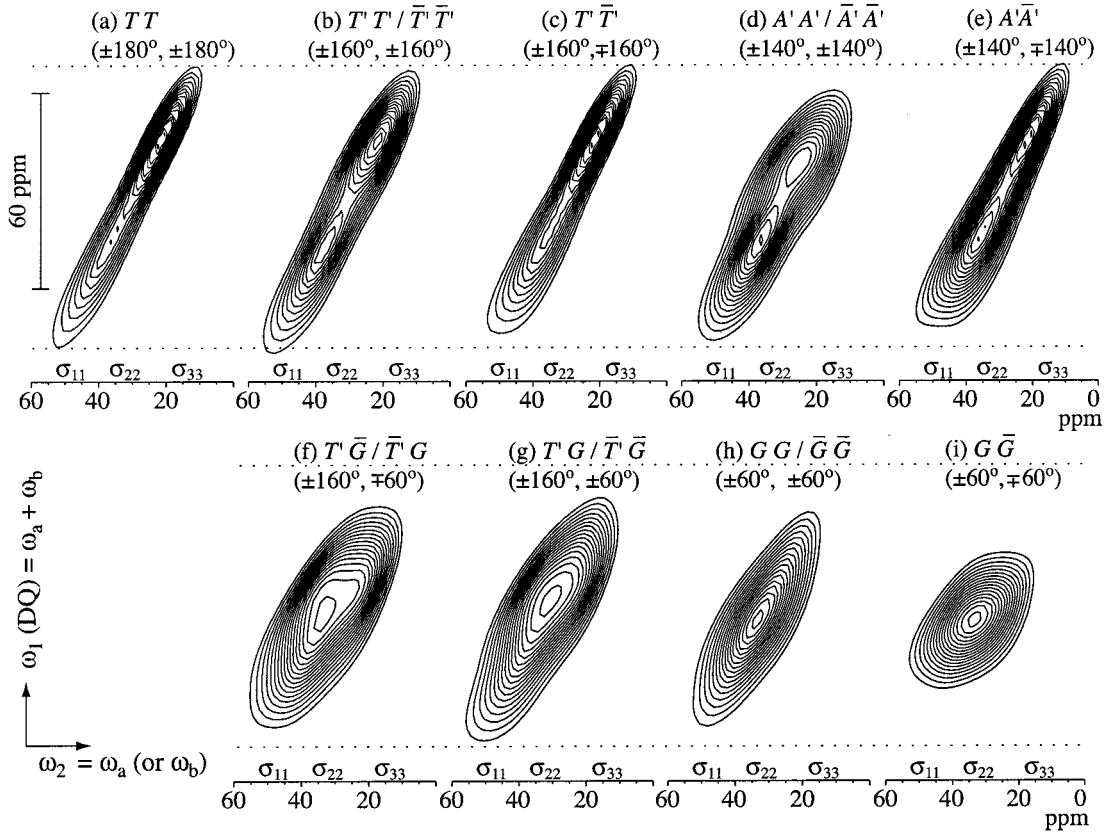

Figure 9. Simulated 2D ^{13}C double-quantum/chemical shift anisotropy spectra of $^{13}CH_2$-aPAN with $^{13}C-^{13}C$ dipolar decoupling (DQ/CSA spectra) for various conformations. The two successive torsion angle values are indicated above each spectrum. Parameters for simulation and plotting are the same as in Figure 6.

$^{13}C-^{13}C$ dipolar coupling as described above. In this experiment, spectra of (±180°, ±180°) and (±160°, ±160°) can be distinguished more clearly from the presence or absence of a central maximum near $\omega_2 = \sigma_{33}$. From the comparison of the experimental and simulated DQ/CSA+CC spectra, it is confirmed that a torsion angle of (±160°, ±160°) is the most suitable angle for simulating the trans conformation in this experiment.

Figure 7b−d shows simulations with trans contents of 90%−70%. In the simulations, torsion angles of (±160°, ±160°) and (160°, 60°) were used for trans−trans and trans−gauche conformations, respectively. As before, the simulated spectrum with a trans content of 70% is wider than the experimental spectrum, and we confirm that the trans content in aPAN is 90% (±10%).

4.3.4. Summary of the Simulations. From the above three experiments, we can conclude that the conformational statistics in aPAN are trans:gauche = 90:10 (±10). The spectra also suggest that the torsion angle of the trans conformation deviates by 20° from the ideal 180° torsion angle. Such a deviation could be due to steric hindrance or electric dipole repulsion of −C≡N groups in meso dyads of aPAN. However, as discussed above, the precise chemical shift tensor orientation cannot be determined for the CH_2 carbon of aPAN. Deviations of the chemical shift tensor orientation from that used for the above simulations will give a similar effect as deviations of the torsion angles. In fact, the chemical shift tensor orientation is expected to depend on the local configuration. The torsion angle of the gauche conformation is expected to deviate from the "ideal" value of ±60° used here.[74] However, the deviations are too small to be resolved in the present experiments, due to the same limitations as discussed for the trans conformations, and also because the fraction of gauche conformers is too small. Since we cannot determine precise torsion angles using the CSA of the $^{13}CH_2$ carbon, distributions of torsion angles were not considered in the above simulations, although distributed torsion angles are suggested in ref 28. Precise analyses of torsion angles and their distributions, by using a $^{13}C\equiv N$-labeled and a $^{13}C/^{2}H$-labeled aPAN sample, will be described in our forthcoming paper.[58] There, the use of the axially symmetric tensors with well-defined orientations along chemical bonds permits detailed torsion angle analyses, in particular for the trans−trans conformations.

4.4. 1D ^{13}C CP/MAS Spectrum. In PE and several other aliphatic polymers, the trans/gauche ratio can be analyzed on the basis of simple 1D ^{13}C MAS spectra and the γ-gauche effect.[83−87] The γ-gauche effect is the decrease of the isotropic chemical shift by 4−6 ppm for each γ-substituent in a gauche conformation. It is, however, only empirical, and we should examine the origin of the isotropic chemical shift change before applying the γ-gauche analysis, since chemical shifts also depend on other effects such as chain packing and configuration. Nevertheless, once the assignment of resonance lines is carried out, we can determine a trans/gauche ratio easily, although detailed torsion angles are not obtained. The aPAN sample does not have γ-carbons in the side groups, which makes the γ-gauche analysis more reliable than for aPS. The various 2D experiments in this paper will check the validity of the γ-gauche analysis for aPAN.

Figure 11a shows the 1D CP/MAS ^{13}C spectrum of the $^{13}CH_2$ units in aPAN. The signal of the overlapping

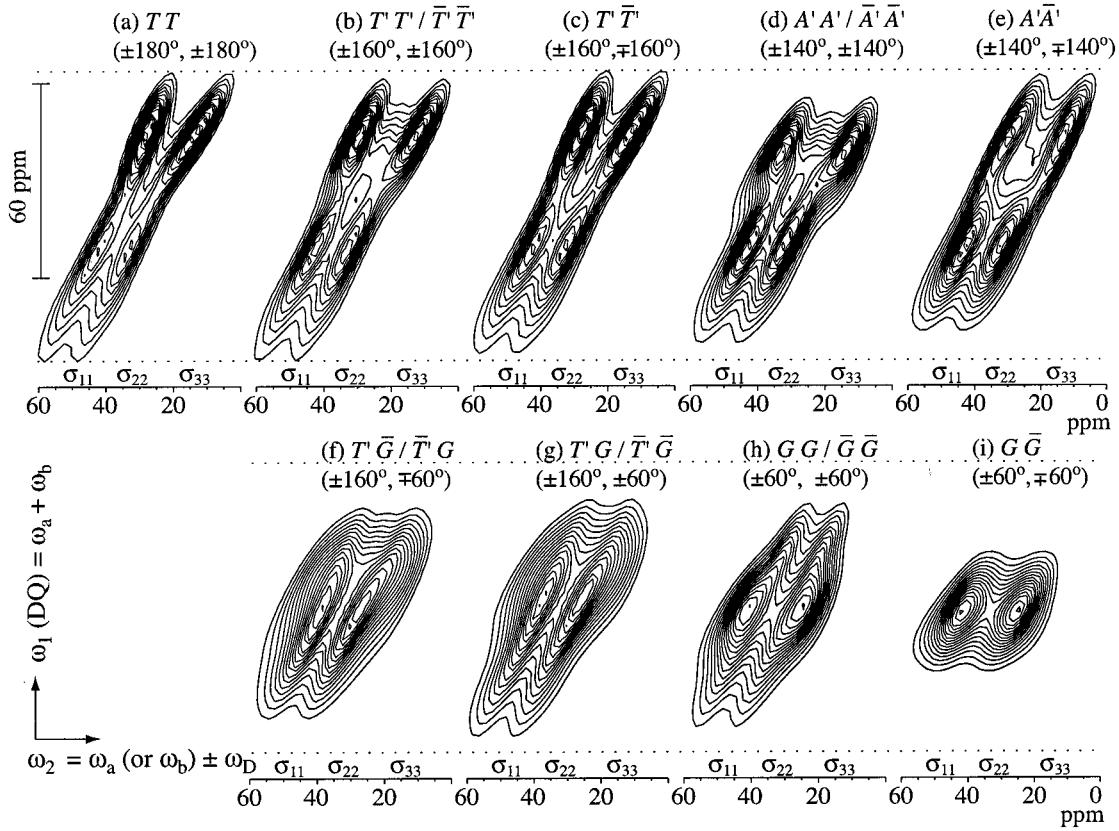

Figure 10. Simulated 2D ^{13}C double-quantum/chemical shift anisotropy spectra of $^{13}CH_2$-aPAN without $^{13}C-^{13}C$ dipolar decoupling (DQ/CSA+CC spectra) for various conformations. The two successive torsion angle values are indicated above each spectrum. Parameters for simulation and plotting are the same as in Figure 7.

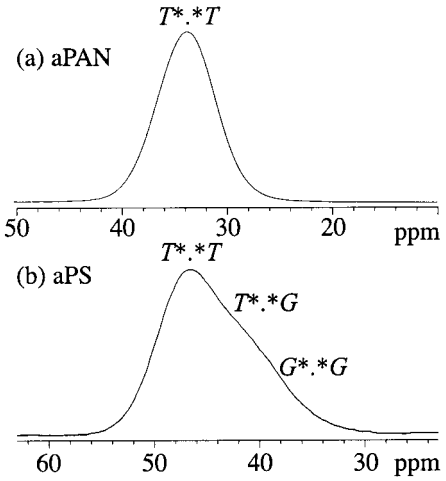

Figure 11. 1D CP/MAS ^{13}C spectra selectively of the methylene groups in (a) $^{13}CH_2$-aPAN and (b) $^{13}CH_2$-aPS. Suggested conformations are indicated for each resonance band.

CH resonance was removed by subtracting the spectrum of an unlabeled aPAN sample from that of the 15% $^{13}CH_2$-aPAN sample, using the natural abundance $^{13}C{\equiv}N$ signals to determine the exact scaling of the subtracted spectrum. The pure $^{13}CH_2$ spectrum exhibits only one peak without any shoulders, suggesting that one conformation is dominant. For comparison, the 1D CP/MAS spectrum of $^{13}CH_2$ units in aPS, whose trans content is 68% (±10%), is shown in Figure 11b. In the spectrum of aPS, we see broad features that can be assigned tentatively to *T*.*T*, *T*.*G*, and *G*.*G* conformations.[55]

These results are consistent with those obtained from the 2D DQF and DQ NMR experiments in this paper and our previous paper,[55] and the resonance line at 33.8 ppm of aPAN can be assigned to a *T*.*T* conformation.

4.5. Comparison with Previous Data. 4.5.1. Trans/Gauche Ratio. In this section, the trans/gauche ratio of aPAN is compared with values proposed in the literature. Grobelny et al.[18] suggested a model with a gauche content of at least 33.3%,[88] which does not agree with our result. The model is based on the purported existence of an isolated proton pair with a distance of 1.5 Å. The distance was calculated from a peak at ~6.5 G, or 55 kHz, in the first-derivative ^1H broad line (BL) NMR spectrum of aPAN at 20 °C. The fallacious conclusion of this approach becomes clear if one considers the ^1H BL-NMR spectrum of polyethylene (PE), where a peak appears at ~7.5 G or 63 kHz,[89] which would correspond to even shorter $^1H-^1H$ distances (1.4 Å). However, such short $^1H-^1H$ distances do not exist in PE, where the geminal H−H distance is 1.8 Å. The additional broadening is due to multispin interactions. Also, in aPAN there is no reason for the proton spin pair to be isolated.

On the basis of Fourier analysis of 2D WAXD patterns of oriented aPAN fibers, Liu and Ruland[20] suggested that the backbone conformation of aPAN is a planar zigzag with a finite persistence length due to interruptions by kinks at irregular intervals. The existence of one kink per 10 monomer units such as a *TGT*$\bar{G}$*T* sequence, which gives an average distance of 2.41 Å per monomer unit along the *c* direction, would reproduce the parallel alignment of chains and the experimental density value. The average distance per monomer unit

along the *c* direction was calculated to be $c = 2.41-2.31$ Å from the experimental density of aPAN, 1.17−1.22 g cm^{-3},[9,32−34] and the nearest chain distance in the pseudohexagonal form, $a = b = \sim 6.0$ Å, from WAXD measurements.[6,9,11,20,28] The gauche content is 10% in this model, which is in good agreement with our results. Moreover, the Liu and Ruland model could successfully explain the diffuse reflection at around 0.3 $Å^{-1}$ without considering an amorphous phase. (The phase structure of aPAN is still controversial, and some authors interpreted this diffuse reflection as an amorphous halo.[16,35,36])

However, Liu and Ruland's model could not explain the full experimental 2D WAXD patterns. The persistence length of 14 Å for the planar zigzag conformation, which was estimated from the width of the meridional reflection, also does not agree with that calculated from one kink per 10 monomer units. We should consider other factors that broaden the WAXD reflections along the chain of aPAN, since one kink per 10 monomer units gives sharper reflections.

Rizzo et al.[28] calculated possible low-energy extended conformations based on a conformational energy minimization procedure. By including trans torsion angles deviating from 180° and distributions of gauche torsion angles, several possible conformers were found that preserve the almost parallel alignment of chains and low conformational energies, without kink formations. In their model, gauche conformations appeared as *TGT* sequences in most cases except for one conformation with *GAGT*. The gauche content in their model can be calculated to be ∼20%, although the value is not given explicitly in ref 28. The average periodicity of the chain in this model is 2.3−2.4 Å, since slight deviations of torsion angles from the exact trans and gauche conformations do not shorten the mean chain periodicity very much. This model was more successful at reproducing the 2D WAXD patterns. The trans/gauche ratio in this model is compatible with our experimental results. The detailed comparison with the torsion angles in this model and their distributions will be addressed in our future paper.[58]

On the basis of ^{2}H NMR line shapes at high temperature (>150 °C), Thomsen et al.[90] suggested a conformation that can undergo a crankshaft motion. They used C−CH_2−C valence bond angles of 114° to explain the ^{2}H NMR spectra. According to the conformational energy minimization calculations by Rizzo et al.,[28] this bond angle may be possible. The ^{2}H spectra indicate that all the C−^{2}H bonds undergo the same motion, which in the crankshaft model gives a gauche content of ∼50%. Because of the difference in temperature, we cannot compare their data directly with ours, but the interpretations will be consistent if the gauche content is greatly increased with increasing temperature. In *trans*-polybutadiene, such an increase in chain disorder has indeed been observed. [91]

A strongly twisted helical structure proposed by Bohn et al.,[9] Rosenbaum,[92] and Henrici-Olivé and Olivé,[14] which gives an average angle of 60−70° between the C≡N (or C−H) bonds and the chain axis,[9] is clearly inconsistent with our experimental findings.

4.5.2. Phase Structure. It is worth noting that the trans/gauche ratio measured by our NMR experiments is for all the components in aPAN. In 1960, Stefani et al.[8] suggested that the planar zigzag crystalline phase in aPAN was composed of syndiotactic sequences by considering the difficulty of trans−trans conformations in isotactic sequences. Hinrichsen[35] estimated a degree of crystallinity of ∼30% by assuming that a broad reflection in the WAXD patterns was an amorphous halo. Even with this low crystallinity, some portion of isotactic sequences would still have to be incorporated into the crystalline phase. In 1993, Hobson and Windle[21,22] showed that isotactic sequences can be incorporated in the crystalline phase, since the isotactic sequences can emulate the shape of the syndiotactic planar zigzag conformation; still, they thought of a two-phase model. Rizzo et al.[28] also showed that meso sequences, at least *m* dyads and *mm* triads, are easily accommodated into the crystalline regions. The models by Rizzo et al.[28] and by Liu and Ruland[20] can explain the broad reflection in the WAXD patterns without assuming the existence of an amorphous phase. The experimental density values are also reproduced without an amorphous phase.

The trans/gauche ratio obtained in our NMR experiments for aPAN as a whole is consistent with that in the crystalline component estimated by Rizzo et al.[28] and Liu and Ruland.[20] If we assumed a two-phase structure, the trans/gauche ratio would be close to 90:10 also for the amorphous region. In other words, the trans/gauche ratios in the crystalline and the amorphous phase would have to be almost the same. This would suggest that the configurational statistics in both phases are similar, and the meso sequences would be predominantly trans−trans even in the amorphous phase. This disproves the original assumption that motivated Stefani et al.[8] to propose an amorphous phase.

In summary, no convincing positive evidence for an amorphous phase in aPAN is currently known. In fact, the high trans content that we found speaks against a significant amorphous phase, since meso trans−trans conformers seem less likely in amorphous regions. This last argument must be regarded with caution, however, since in PE the conformations in the amorphous phase are predominantly trans at low temperatures, because the trans state is energetically more favored than the gauche state.[93] This indicates that it may be problematic to try to identify the phase structure only from the backbone conformation. Information on the phase structure extracted from dynamics measurements will be discussed in our forthcoming paper.[58]

5. Conclusions

The conformational statistics of the backbone bonds in aPAN were investigated by 2D double-quantum filtered CC/CSA as well as ^{13}C-coupled and ^{13}C-decoupled double-quantum solid-state NMR experiments, using a 15% $^{13}CH_2$-labeled aPAN sample. From the NMR spectra, the trans/gauche ratio was determined to be 90%:10% (±10%). This value is consistent with the previously reported density and WAXD patterns of aPAN. The chemical shift tensor orientation of the CH_2 carbon, which must be known in the simulations of the double-quantum spectra, was determined using 2D CH/CSA and HH/CSA correlation experiments. The orientation of the principal axes with respect to the chemical bonds is the same as that of the CH_2 carbons of polyethylene and atactic polystyrene, within ±20°. The validity of the γ-gauche analysis of the isotropic chemical shift of the CH_2 site in aPAN was examined by analyzing the 1D CP/MAS ^{13}C spectrum of the 15%

$^{13}CH_2$-labeled aPAN in view of the above-mentioned 2D NMR results. The single CP/MAS resonance line at 33.8 ppm was assigned to the *T**.**T* conformation.

Acknowledgment. H.K. thanks the International Fellowship by the Ministry of Education, Science, Sports and Culture, Japan, for financial support. K.S.R. thanks the National Science Foundation (DMR 9703916) for funding this work and NSF/MRSEC for support of the NMR facility.

References and Notes

(1) Tadokoro, H. *Structure of Crystalline Polymers*; J. Wiley & Sons: New York, 1979.
(2) Schaefer, J. *Macromolecules* **1971**, *4*, 105.
(3) Kamide, K.; Yamazaki, H.; Okajiama, K.; Hikichi, K. *Polym. J.* **1985**, *17*, 1291.
(4) Kamide, K.; Yamazaki, H.; Okajiama, K.; Hikichi, K. *Polym. J.* **1985**, *17*, 1233.
(5) Some atactic vinyl polymers with small side groups, such as atactic polypropylene, cannot crystallize.
(6) Natta, G.; Mazzanti, G.; Corradini, P. *Atti Accad. Naz. Lincei, Cl. Sci. Fis., Mat. Nat., Rend.* **1958**, *25*, 3.
(7) Krigbaum, W. R.; Tokita, N. *J. Polym. Sci.* **1960**, *43*, 467.
(8) Stefani, R.; Chevreton, M.; Garnier, M.; Eyraud, C. *Compt. Rend.* **1960**, *251*, 2174.
(9) Bohn, C. R.; Schaefgen, J. R.; Statton, W. O. *J. Polym. Sci.* **1961**, *55*, 531.
(10) Holland, V. F.; Mitchell, S. B.; Hunter, W. L.; Lindenmeyer, P. H. *J. Polym. Sci.* **1962**, *62*, 145.
(11) Lindenmeyer, P. H.; Hosemann, R. *J. Appl. Phys.* **1963**, *34*, 42.
(12) Klement, J. J.; Geil, P. H. *J. Polym. Sci., Polym. Phys. Ed.* **1968**, *6*, 1381.
(13) Colvin, B. G.; Storr, P. *Eur. Polym. J.* **1974**, *10*, 337.
(14) Henrici-Olive, G.; Olive, S. *Adv. Polym. Sci.* **1979**, *32*, 125.
(15) Hinrichsen, G.; Orth, H. *Kolloid-Z. Z. Polym.* **1971**, *247*, 844.
(16) Gupta, A. K.; Chand, N. *Eur. Polym. J.* **1979**, *15*, 899.
(17) Gupta, A. K.; Singhal, R. P.; Agarwal, V. K. *Polymer* **1981**, *22*, 285.
(18) Grobelny, J.; Tekely, P.; Turska, E. *Polymer* **1981**, *22*, 1649.
(19) Gupta, A. K.; Maiti, A. K. *J. Appl. Polym. Sci.* **1982**, *27*, 2409.
(20) Liu, X. D.; Ruland, W. *Macromolecules* **1993**, *26*, 3030.
(21) Hobson, R. J.; Windle, A. H. *Polymer* **1993**, *34*, 3582.
(22) Hobson, R. J.; Windle, A. H. *Macromolecules* **1993**, *26*, 6903.
(23) Mathieu, D.; Defranceschi, M.; Lecayon, G.; Grand, A.; Delhalle, J. *Chem. Phys.* **1993**, *171*, 133.
(24) Mathieu, D.; Defranceschi, M.; Lecayon, G.; Delhalle, J. *Chem. Phys.* **1994**, *188*, 183.
(25) Bashir, Z. *J. Polym. Sci., Part B: Polym. Phys.* **1994**, *32*, 1115.
(26) Allen, R. A.; Ward, I. M.; Bashir, Z. *Polymer* **1994**, *35*, 2063.
(27) Allen, R. A.; Ward, I. M.; Bashir, Z. *Polymer* **1994**, *35*, 4035.
(28) Rizzo, P.; Auriemma, F.; Guerra, G.; Petraccone, V.; Corradini, P. *Macromolecules* **1996**, *29*, 8852.
(29) Yamane, A.; Sawai, D.; Kameda, T.; Kanamoto, T.; Ito, M.; Porter, R. S. *Macromolecules* **1997**, *30*, 4170.
(30) Sawai, D.; Kanamoto, T.; Porter, R. S. *Macromolecules* **1998**, *31*, 2010.
(31) Sawai, D.; Yamane, A.; Takahashi, H.; Kanamoto, T.; Ito, M.; Porter, R. S. *J. Polym. Sci., Part B: Polym. Phys.* **1998**, *36*, 629.
(32) Stefani, R.; Chevreton, M.; Terrier, J.; Eyraud, C. *Compt. Rend.* **1959**, *248*, 2006.
(33) Chiang, J. *J. Polym. Sci., Part A* **1963**, *1*, 2765.
(34) Chiang, J. *J. Polym. Sci., Part A* **1965**, *3*, 2109.
(35) Hinrichsen, G. *J. Polym. Sci.* **1972**, *C38*, 303.
(36) Gupta, A. K.; Singhal, R. P. *J. Polym. Sci., Polym. Phys. Ed.* **1983**, *21*, 2243.
(37) Edzes, H. T.; Bernards, J. P. C. *J. Am. Chem. Soc.* **1984**, *106*, 1515.
(38) Henrichs, P. M.; Linder, M. *J. Magn. Reson.* **1984**, *58*, 458.
(39) Tycko, R.; Dabbagh, G. *J. Am. Chem. Soc.* **1991**, *113*, 3592.
(40) Robyr, P.; Meier, B. H.; Ernst, R. R. *Chem. Phys. Lett.* **1991**, *187*, 471.
(41) Robyr, P.; Meier, B. H.; Fischer, P.; Ernst, R. R. *J. Am. Chem. Soc.* **1994**, *116*, 5315.
(42) Dabbagh, G.; Weliky, D. P.; Tycko, R. *Macromolecules* **1994**, *27*, 6183.
(43) Robyr, P.; Tomaselli, M.; Grob-Pisano, C.; Meier, B. H.; Ernst, R. R.; Suter, U. W. *Macromolecules* **1995**, *28*, 5320.
(44) Robyr, P.; Tomaselli, M.; Straka, J.; Grob-Pisano, C.; Suter, U. W.; Meier, B. H.; Ernst, R. R. *Mol. Phys.* **1995**, *84*, 995.
(45) Kummerlen, J.; van Beek, J. D.; Vollrath, F.; Meier, B. H. *Macromolecules* **1996**, *29*, 2920.
(46) Robyr, P.; Utz, M.; Gan, Z.; Scheurer, C.; Tomaselli, M.; Suter, U. W.; Ernst, R. R. *Macromolecules* **1998**, *31*, 5818.
(47) Robyr, P.; Gan, Z.; Suter, U. W. *Macromolecules* **1998**, *31*, 8918.
(48) Robyr, P.; Gan, Z.; Suter, U. W. *Macromolecules* **1998**, *31*, 6199.
(49) Robyr, P.; Gan, Z. *J. Magn. Reson.* **1998**, *131*, 254.
(50) Kaji, H.; Horii, F. *J. Chem. Phys.* **1998**, *109*, 4651.
(51) Schmidt-Rohr, K. *Macromolecules* **1996**, *29*, 3975.
(52) Schmidt-Rohr, K. *J. Am. Chem. Soc.* **1996**, *118*, 7601.
(53) Schmidt-Rohr, K. *J. Magn. Reson.* **1998**, *131*, 209.
(54) Schmidt-Rohr, K.; Hu, W.; Zumbulyadis, N. *Science* **1998**, *280*, 714.
(55) Dunbar, M. G.; Novak, B. M.; Schmidt-Rohr, K. *Solid State Nucl. Magn. Reson.* **1998**, *12*, 119.
(56) Utz, M. *J. Chem. Phys.* **1998**, *109*, 6110.
(57) Harris, D. J.; Bonagamba, T. J.; Schmidt-Rohr, K. *Macromolecules* **1999**, *32*, 6718.
(58) Kaji, H.; Schmidt-Rohr, K., to be submitted to *Macromolecules*.
(59) Wilkinson, W. K. *Macromolecular Syntheses*; John Wiley & Sons: New York, 1977; Vol. 1.
(60) Brandrup, J.; Immergut, E. H. *Polymer Handbook*; John Wiley & Sons: New York, 1989.
(61) Shibukawa, T.; Sone, M.; Uchida, A.; Iwahori, K. *J. Polym. Sci., Part A-1* **1968**, *6*, 147.
(62) Dunbar, M. G.; Kaji, H.; de Azevedo, E. R.; Bonagamba, T. J.; Schmidt-Rohr, K., to be submitted to *Macromolecules*.
(63) Kaji, H.; Schmidt-Rohr, K., to be submitted to *Macromolecules*.
(64) Haeberlen, U. *High-Resolution NMR in Solids*; Academic Press: New York, 1976; Vol. 1.
(65) Mehring, M. *Principle of High-Resolution NMR in Solids*, 2nd ed.; Springer: Berlin, 1984.
(66) Linder, M.; Hohener, A.; Ernst, R. R. *J. Chem. Phys.* **1980**, *73*, 4959.
(67) Terao, T.; Miura, H.; Saika, A. *J. Chem. Phys.* **1986**, *85*, 3816.
(68) Nakai, T.; Ashida, J.; Terao, T. *J. Chem. Phys.* **1988**, *88*, 6049.
(69) Schmidt-Rohr, K.; Wilhelm, M.; Johansson, A.; Spiess, H. W. *Magn. Reson. Chem.* **1993**, *31*, 352.
(70) Schmidt-Rohr, K.; Spiess, H. W. *Multidimensional Solid-State NMR and Polymers*; Academic Press: London, 1994.
(71) Kaji, H.; Schmidt-Rohr, K., submitted to *Appl. Magn. Reson.*
(72) IUPAC Commission on Macromolecular Nomenclature. *Pure Appl. Chem.* **1980**, *53*, 733.
(73) Flory, P. J.; Fujiwara, Y. *Macromolecules* **1969**, *2*, 315.
(74) Flory, P. J.; Jackson, J. G.; Wood, C. J. *Statistical Mechanics of Chain Molecules*, 2nd ed.; Oxford University Press: New York, 1989.
(75) Mattice, W. L.; Suter, U. W. *Conformational Theory of Large Molecules: The Rotational Isomeric State Model in Macromolecular Systems*; Wiley: New York, 1994.
(76) Ernst, R. R.; Bodenhausen, G.; Wokaun, A. *Principles of Nuclear Magnetic Resonance in One and Two Dimensions*; Clarendon Press: Oxford, 1987.
(77) VanderHart, D. L. *J. Chem. Phys.* **1976**, *64*, 830.
(78) Opella, S. J.; Waugh, J. S. *J. Chem. Phys.* **1977**, *66*, 4919.
(79) Tomaselli, M.; Robyr, P.; Meier, B. H.; Grob-Pisano, C.; Ernst, R. R.; Suter, U. W. *Mol. Phys.* **1996**, *89*, 1663.
(80) Tomaselli, M.; Zehnder, M. M.; Robyr, P.; Grob-Pisano, C.; Ernst, R. R.; Suter, U. W. *Macromolecules* **1997**, *30*, 3579.
(81) In 2D DQ experiments, $\omega_1 = \omega_a + \omega_b$, $\omega_2 = \omega_a$ or ω_b. On the diagonal of slope two, $\omega_1 = 2\omega_2$. These relations result in $\omega_a = \omega_b$. Details of the relation between 2D DQ and 2D CSA spin diffusion experiments are described in ref 53.
(82) Nakai, T.; McDowell, C. A. *Mol. Phys.* **1993**, *79*, 965.
(83) Bovey, F. A. *Chain Structure and Conformation of Macromolecules*; Academic Press: New York, 1982.
(84) Tonelli, A. E. *NMR Spectroscopy and Polymer Microstructure: The Conformational Connection*; VCH Publishers: New York, 1989.
(85) Zemke, K.; Schmidt-Rohr, K.; Spiess, H. W. *Acta Polym.* **1994**, *45*, 148.
(86) Ishida, H.; Kaji, H.; Horii, F. *Macromolecules* **1997**, *30*, 5799.
(87) Born, R.; Spiess, H. W. *Ab initio Calculations of Conformational Effects on ^{13}C NMR spectra of Amorphous Polymers*; Spring Verlag: Berlin, 1997; Vol. 35.

(88) To incorporate 16.6% of protons in special pairs, all the iso- and heterotactic triads should take their proposed special conformations; -*-*T*-*G*-*G*-*T*- for iso- and -*-*T*-*G*-*G*-*G*- for heterotactic triads. This leads to at least 33.3% of gauche.
(89) Smith, J. B.; Manuel, A. J.; Ward, I. M. *Polymer* **1975**, *16*, 57.
(90) Thomsen, T.; Zachmann, H. G.; Korte, S. *Macromolecules* **1992**, *25*, 6934.
(91) Schilling, F. C.; Gomez, M. A.; Tonelli, A. E.; Bovey, F. A.; Woodward, A. E. *Macromolecules* **1987**, *20*, 2954.
(92) Rosenbaum, S. *J. Appl. Polym. Sci.* **1965**, *9*, 2071, 2085.
(93) Ando, I.; Yamanobe, T.; Akiyama, S.; Komoto, T.; Sato, H.; Fujito, T.; Deguchi, K.; Imanari, M. *Solid State Commun.* **1987**, *62*, 785.

MA0002592